Surface Electric Fields and Impedance Matrix Elements of Stratified Media

Leung Tsang, *Fellow, IEEE*, Chung-Chi Huang, and Chi Hou Chan

***Abstract*—For the various geometrical configurations of waves in stratified media, we consider the important case when both source and field points are located on the same interface separating two different dielectric media. We shall denote this configuration as surface electric field case. In this paper, the electric fields are calculated numerically without using potentials. For the surface electric field case the integrand of the electric field grows with $k_\rho^{3/2}$ for large k_ρ making the Sommerfeld integral singular. To calculate the surface electric fields in the spatial domain, we recently applied a technique of higher order asymptotic extraction. In the higher order asymptotic extraction, the higher order asymptotic parts were calculated analytically. The remainder, which has an integrand decays as $k_\rho^{-3/2}$, was calculated numerically along the Sommerfeld contour path of integration. In this paper, we use a different extraction technique, the half-space extraction. After the half-space extraction, the integrand of the Sommerfeld integral of stratified media decays exponentially and the integral is calculated along the Sommerfeld integration path. The half-space extraction part is calculated by numerical integration along the vertical branch cuts. The surface electric fields for stratified media using half-space extraction and higher order asymptotic extraction are in good agreement. To validate the accuracy of the solution, we also compute the impedance matrix elements using surface electric fields, testing, and basis functions all in spatial domain. The results are then compared with the results of the spectral domain method. The comparisons of the complex impedance matrix elements are tabulated and show that the difference is less than 2%.**

***Index Terms*—Integral equation methods, method of moments (MoM), nonhomogeneous media.**

I. Introduction

We present this paper in memory of Prof. James R. Wait for his pioneering work in the research of stratified media. Radiation of waves in stratified media were studied extensively, beginning during the time of Prof. Wait, for application in geophysical probing [1]–[4]. He evaluated the Sommerfeld integrals by contour integration, asymptotic methods, and the use of vertical branch cuts [3]. He also calculated near-field static and quasi-static solutions [1]–[4]. For the half-space case, the vertical branch cuts were also selected with a result that the Zenneck surface wave pole lies on the lower Riemann sheet [3], [5]. Subsequently, numerical methods are used to evaluate the Sommerfeld integrals [3], [6]–[8]. Recently, the problem of waves in stratified media has also important applications in microstrip structures [9]. The evaluation of the impedance matrix elements for the electric field integral equation is an important step in such problems.

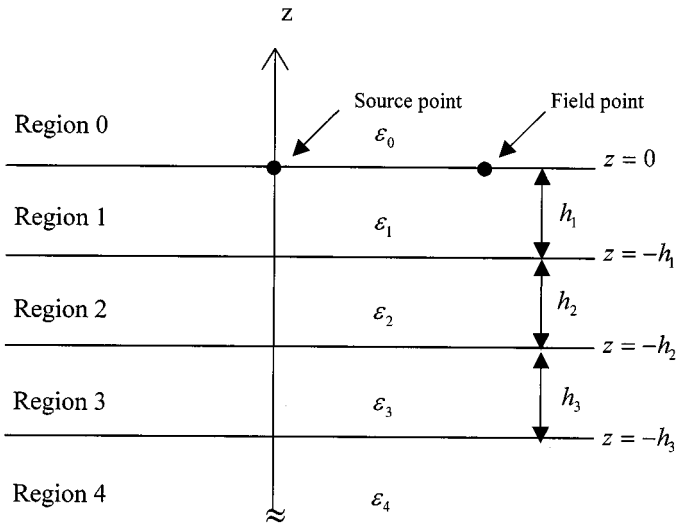

Fig. 1. A stratified media. The unit dyadic point source is at the origin on the surface.

For the various geometrical configurations of waves in stratified media, the important case is when both source and field points are located on the same interface separating two different dielectric media as shown in Fig. 1. We shall denote this configuration as the surface electric field case and shall exclusively address this case. For geophysical probing, this configuration will have the maximum effect of subsurface properties. For microstrip structures, this configuration is common. However, for this configuration, the integrand of Sommerfeld integral does not have exponential decay for large k_ρ. The integrand of the electric field actually grows with $k_\rho^{3/2}$ for large k_ρ making the Sommerfeld integral singular. To circumvent the difficulty, potentials such as Hertz potentials and mixed potentials [1]–[4], [8], [9] are used because the integrands are less singular. Techniques such as complex image method are also used [10]–[13]. This leads to the mixed potential integral equation (MPIE)[9] in the spatial domain for calculating current distribution on stratified media. Impedance matrix elements are calculated using mixed potentials. An alternative is to use spectral domain method [14]. In this case, the Fourier transforms of the testing and basis function are incorporated into Sommerfeld integrals. This makes the integrand decay for large k_ρ.

For practical applications, it is useful to calculate the surface electric fields in the spatial domain. First, the electric fields are

Manuscript received August 19, 1999; revised January 31, 2000.

L. Tsang and C.-C. Huang are with the Department of Electrical Engineering, University of Washington, Seattle, WA 98195-2500 USA (e-mail: tsang1@u.washington.edu).

C. H. Chan is with the Department of Electronic Engineering, City University of Hong Kong, Kowloon, Hong Kong.

Publisher Item Identifier S 0018-926X(00)09342-X.

measurable in experiments. Second, the electric fields have a simple cosine/sine dependence on the ϕ coordinate. Once calculated, the ρ dependence can be tabulated. The electric fields for variousρ and ϕ can be easily retrieved by the lookup table. For the case of impedance matrix elements, they can be calculated readily by using the tabulated values and simple quadrature over the spatial extent of the subsectional basis and testing functions.

To calculate the surface electric fields in the spatial domain and to deal with the $k_\rho^{3/2}$ growth in the integrand of the Sommerfeld integral, we recently applied a technique of higher order asymptotic extraction [15], [16]. In the higher order asymptotic extraction, the asymptotic parts were calculated analytically. The remainder which decays as $k_\rho^{-3/2}$ was calculated numerically along the Sommerfeld contour path of integration. The integration path in Fig. 2 is referred to as "Sommerfeld integration path" because the original path of integration was identified by Sommerfeld in his book [17]. Miller actually did the numerical integration along the contour [18]. The results were illustrated for stratified media [15], [16]. In this paper, we use a different extraction technique—the half-space extraction. After the half-space extraction, the integrand of Sommerfeld integral of stratified media decays exponentially and the integral is calculated along the Sommerfeld integration paths. The half-space extraction part is calculated by numerical integration along the vertical branch cuts [1], [5], [7]. The surface electric fields are calculated for stratified media. In a related work using the extraction technique, Tsalamengas studied the problem of TE-scattering by conducting strips right on the dielectric interface [19]. In this paper, the approach is on the use of the spatial domain electric field Green's function without using the potentials. Also, an efficient approach for the evaluation of the Sommerfeld integral associated with half-space was describe by Michalski [20]. We note that in the presented method, the computation time is dominated by the nonhalf-space solution part. The half-space solution itself only accounts for a small portion of the total computation time. The results of half-space extraction and higher order asymptotic extraction are in good agreement. In these two procedures of calculating surface electric fields for stratified media, the location of poles are not required. The use of potentials is not required, either. To validate the accuracy of the solution, we also compute the impedance matrix elements using electric field, testing, and basis functions all in spatial domain. The results are then compared with the results of the spectral domain method [14]. The comparisons are tabulated and show that the difference is less than 2%.

In Section II, we give the formulation of the electric field spatial Green's functions for stratified media. In Section III, we describe the solution of surface electric field using the half-space extraction technique. In Section IV, we briefly summarize the results of the higher order asymptotic extraction technique. In Section V, numerical results are shown for the computed surface electric fields up to 1.5 free-space wavelengths. It is shown that the results computed with half-space extraction and higher order asymptotic extraction are in good agreement. In Section VI, the results of impedance elements are presented up to a separation distance of 1.5 free-space wavelengths. Comparisons are made between the present method (surface electric field in the spatial domain) and the spectral domain method showing that the difference is less than 2%.

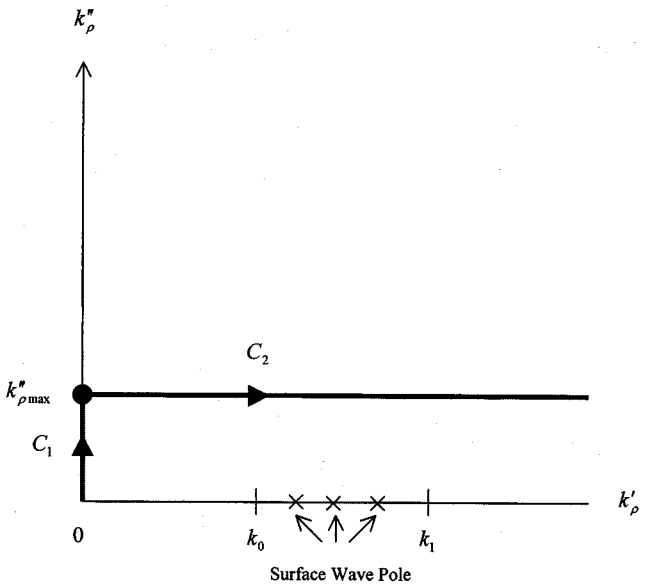

Fig. 2. Sommerfeld contour integration path used in numerical integration, $C_s = C_1 + C_2$.

II. Evaluation of the Electric Fields of the Spatial Green's Functions on the Surface

Consider a stratified media as shown in Fig. 1. The electric field spatial domain Green's function with source and observation point on the surface of the dielectric substrate can be expressed by

$$G_{xx}(X, Y) = W_\rho(\rho)\cos^2\phi - W_\phi(\rho)\sin^2\phi \tag{1}$$

where

$$\rho = \sqrt{X^2 + Y^2} \quad \text{and} \quad \phi = \tan^{-1}\left(\frac{Y}{X}\right) \tag{2}$$

$$W_\rho(\rho) = \lim_{z\to 0^+}\frac{-1}{4\pi\omega\varepsilon_0} \cdot\left\{\int_{C_s} dk_\rho k_\rho k_z(1-R_{\rm TM})J_1'(k_\rho\rho)e^{-jk_z z} + \frac{k_0^2}{\rho}\int_{C_s} dk_\rho(1+R_{\rm TE})\frac{J_1(k_\rho\rho)}{k_z}e^{-jk_z z}\right\} \tag{3}$$

$$W_\phi(\rho) = \lim_{z\to 0^+}\frac{1}{4\pi\omega\varepsilon_0} \cdot\left\{\frac{1}{\rho}\int_{C_s} dk_\rho k_z(1-R_{\rm TM})J_1(k_\rho\rho)e^{-jk_z z} + k_0^2\int_{C_s} dk_\rho(1+R_{\rm TE})\frac{k_\rho J_1'(k_\rho\rho)}{k_z}e^{-jk_z z}\right\}. \tag{4}$$

The $e^{-jk_z z}$ is included in (3) and (4) for the definition of the integration. It will be suppressed from now on. Because the source and field points are at the same interface, the integrand does not have exponential decay. The integrand grows with $k_\rho^{3/2}$. The Green's function$G_{xx}(X, Y)$ represents the $\hat{x}$ component of electric field due to an infinitesimal $\hat{x}$-directed current source.

Note that W_ρ and W_ϕ only depend on ρ. Thus they can be calculated as a function of ρ and tabulated. Then for a given X and Y, $G_{xx}(X, Y)$ can be readily calculated by using (1). In (3) and (4), C_s is the Sommerfeld Integration path as shown in Fig. 2. The reflection coefficients of the stratified media are represented by $R_{\rm TM}$ and $R_{\rm TE}$, respectively, for TM and TE waves. For the case of the source point on the surface of the stratified media [17]–[19], reflection coefficients are calculated using the recurrence relationship

$$\frac{A_l}{B_l}e^{2jk_{lz}h_l} = \frac{\dfrac{A_{(l+1)}}{B_{(l+1)}}e^{2jk_{(l+1)z}h_{(l+1)}}\cdot e^{-2jk_{(l+1)z}(h_{(l+1)}-h_l)}+R^{\rm TM\,or\,TE}_{l(l+1)}}{\dfrac{A_{(l+1)}}{B_{(l+1)}}e^{2jk_{(l+1)z}h_{(l+1)}}\cdot R^{\rm TM\,or\,TE}_{l(l+1)}\cdot e^{-2jk_{(l+1)z}(h_{(l+1)}-h_l)}+1} \tag{5}$$

where

$$R^{\rm TE}_{l(l+1)} = \frac{k_{lz}-k_{(l+1)z}}{k_{lz}+k_{(l+1)z}}, \quad R^{\rm TM}_{l(l+1)} = \frac{\varepsilon_{l+1}k_{lz}-\varepsilon_l k_{(l+1)z}}{\varepsilon_{l+1}k_{lz}+\varepsilon_l k_{(l+1)z}} \tag{6}$$

and $k_{lz}=\sqrt{k_l^2-k_\rho^2}$, $k_l=\omega\sqrt{\mu_0\varepsilon_l}$, $k_0=\omega\sqrt{\mu_0\varepsilon_0}$, h_i is the layer thickness of the ith layer.

Because of singularities on the real k_ρ axis, the integration is carried out on the Sommerfeld integration path C_s, which passes the origin and lies in the first quadrant asymptotically parallel to the real k_ρ axis. The complex variable k_ρ has real and imaginary parts denoted by k'_ρ and k''_ρ, respectively. In the numerical integration that is performed in this paper, we have chosen the line contour integrals of C_1 and C_2, as shown in Fig. 2, so that $C_s = C_1 + C_2$. On C_1, $k_\rho = jk''_\rho$ with $0 \le k''_\rho \le k''_{\rho\max}$. On C_2, $k_\rho = k'_\rho + jk''_{\rho\max}$, with $0 \le k'_\rho \le \infty$. However, because of the $k_\rho^{3/2}$ growth of the integrand, numerical integration can only be done after extraction as illustrated in the following sections.

After extraction, the choices of numerical parameters in this paper are $k''_{\rho\max} = 0.1/h$ and the step size $\Delta k''_\rho = \Delta k'_\rho = \min(0.1k''_{\rho\max},\, 0.05/\rho,\, 0.01k_0)$ along C_1 and C_2, respectively. Along C_2 we integrate up to $k'_{\rho\max} = \max(10/h,\, 15k_1)$.

III. Evaluation of Surface Electric Field Spatial Green's Function Using Half-Space Extraction

In the method of half-space extraction, we have

$$\begin{aligned} R_{\rm TM} &= (R_{\rm TM} - R^{\rm TM}_{01}) + R^{\rm TM}_{01} \\ R_{\rm TE} &= (R_{\rm TE} - R^{\rm TE}_{01}) + R^{\rm TE}_{01} \end{aligned} \tag{7}$$

$R^{\rm TM}_{01}$ and $R^{\rm TE}_{01}$ represents half-space solution, $R_{\rm TM} - R^{\rm TM}_{01}$ and $R_{\rm TE} - R^{\rm TE}_{01}$ represents remainder after half-space extraction.

Thus

$$W_{\rho\,{\rm or}\,\phi}(\rho) = W^{(N)}_{\rho\,{\rm or}\,\phi}(\rho) + W^{(H)}_{\rho\,{\rm or}\,\phi}(\rho) \tag{8}$$

where (N) denotes numerical and (H) denotes half-space. The half-space is evaluated by using the two vertical branch cuts as shown in Fig. 3.

$$W^{(H)}_{\rho\,{\rm or}\,\phi}(\rho) = W^{(H,\,BC0)}_{\rho\,{\rm or}\,\phi}(\rho) + W^{(H,\,BC1)}_{\rho\,{\rm or}\,\phi}(\rho) \tag{9}$$

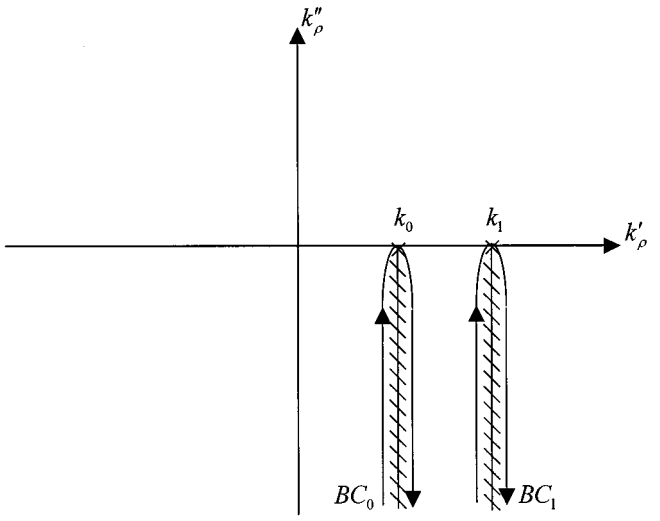

Fig. 3. Integration contour of the branch cuts for the half-space solution as a result of half-space extraction.

where $BC0$ represents vertical branch cut associated with k_0 and $BC1$ represents the vertical branch cut associated with k_1. Thus

$$W_\rho(\rho) = W^{(N)}_\rho(\rho) + W^{(H,\,BC0)}_\rho(\rho) + W^{(H,\,BC1)}_\rho(\rho) \tag{10}$$

$$W_\phi(\rho) = W^{(N)}_\phi(\rho) + W^{(H,\,BC0)}_\phi(\rho) + W^{(H,\,BC1)}_\phi(\rho) \tag{11}$$

where

$$W^{(N)}_\rho(\rho) = \frac{-1}{4\pi\omega\varepsilon_0}\left\{\int_{Cs} dk_\rho k_\rho k_z \left(R^{\rm TM}_{01} - R_{\rm TM}\right) J'_1(k_\rho\rho) + \frac{k_0^2}{\rho}\int_{Cs} dk_\rho \left(R_{\rm TE} - R^{\rm TE}_{01}\right)\frac{J_1(k_\rho\rho)}{k_z}\right\}. \tag{12}$$

The integrand decay exponentially for large k_ρ after half-space extraction. The half-space solution can be calculated by integration along the two branch cuts $BC0$ and $BC1$. Although the integrand of the half-space solution grows with k_ρ, the results of the integration actually exists (Appendix I). For the half-space problem, there is no pole of $R^{\rm TM}_{01}$ in the upper Riemann sheet if vertical branch cuts are used [3], [5].

For $BC0$, which is the branch cut of k_z

$$W^{(H,\,BC0)}_\rho(\rho) = \frac{-1}{4\pi\omega\varepsilon_0}\left\{-\int_{-\infty}^{{\rm Im}_{k_0}} j\,dk''_\rho \frac{2k_\rho k^2_{1z}(k_z)_R}{k^2_{1z}-(\varepsilon_r(k_z)_R)^2}H^{(2)}_1(k_\rho\rho) + \frac{k_0^2}{\rho}\int_{-\infty}^{{\rm Im}_{k_0}} j\,dk''_\rho \frac{2(k_z)_R}{k^2_{1z}-((k_z)_R)^2}H^{(2)}_1(k_\rho\rho)\right\} \tag{13}$$

where $\varepsilon_r = \varepsilon_1/\varepsilon_0$.

In (13), $k_\rho = k + jk''_\rho$ where k''_ρ runs from $-\infty$ to 0. In (13), $(k_z)_R$ is the value of $k_z$on the right side of the branch cut. If we use $(k_z)_L$ to denote the value of k_z on the left side of the branch cut, then $(k_z)_R = -(k_z)_L$. On $BC0$, ${\rm Re}(k_z)_R < 0$ and ${\rm Im}(k_z)_R < 0$. Also on $BC0$ in (13), ${\rm Re}(k_{1z})_R > 0$ and

$\mathrm{Im}(k_{1z})_R > 0$. Note also that Hankel function of the second kind is in the integrand of branch cut integration. On $BC1$, which is the branch cut for k_{1z}

$$W_\rho^{(H,\,BC1)}(\rho) = \frac{-1}{4\pi\omega\varepsilon_0}\left\{-\int_{-\infty}^{\mathrm{Im}k_1} j\,dk_\rho'' \frac{2\varepsilon_r k_\rho k_z^2 (k_{1z})_R}{(\varepsilon_r k_z)^2 - ((k_{1z})_R)^2} H_1'^{(2)}(k_\rho\rho) + \frac{k_0^2}{\rho}\int_{-\infty}^{\mathrm{Im}k_1} j\,dk_\rho'' \frac{2(k_{1z})_R}{k_z^2 - ((k_{1z})_R)^2} H_1^{(2)}(k_\rho\rho)\right\}. \tag{14}$$

On $BC1$, $k_\rho = k_1 + jk_\rho''$ where k_ρ'' runs from $-\infty$ to $\mathrm{Im}(k_1)$. In (14), $(k_z)_R = -(k_z)_L$, where R and L denote the right side and left side of $BC1$, respectively. We have $\mathrm{Re}(k_{1z})_R < 0$ and $\mathrm{Im}(k_{1z})_R < 0$. Also on $BC1$ in (2), $\mathrm{Im}(k_z) < 0$. Integrals in (13) and (14) can be solved numerically for nonzero ρ. Similarly, for $W_\phi(\rho)$ we have

$$W_\phi^{(N)}(\rho) = \frac{1}{4\pi\omega\varepsilon_0}\left\{\frac{1}{\rho}\int_{Cs} dk_\rho k_z (R_{01}^{\mathrm{TM}} - R_{\mathrm{TM}}) J_1(k_\rho\rho) + k_0^2 \int_{Cs} dk_\rho k_\rho (R_{\mathrm{TE}} - R_{01}^{\mathrm{TE}}) \frac{J_1'(k_\rho\rho)}{k_z}\right\} \tag{15}$$

$$W_\phi^{(H,\,BC0)}(\rho) = \frac{1}{4\pi\omega\varepsilon_0}\left\{-\frac{1}{\rho}\int_{-\infty}^{\mathrm{Im}k_0} j\,dk_\rho'' \frac{2k_{1z}^2 (k_z)_R}{k_{1z}^2 - (\varepsilon_r (k_z)_R)^2} H_1^{(2)}(k_\rho\rho) + k_0^2 \int_{-\infty}^{\mathrm{Im}k_0} j\,dk_\rho'' \frac{2k_\rho (k_z)_R}{k_{1z}^2 - ((k_z)_R)^2} H_1'^{(2)}(k_\rho\rho)\right\} \tag{16}$$

$$W_\phi^{(H,\,BC1)}(\rho) = \frac{1}{4\pi\omega\varepsilon_0}\left\{-\frac{1}{\rho}\int_{-\infty}^{\mathrm{Im}k_1} j dk_\rho'' \frac{2\varepsilon_r k_z^2 (k_{1z})_R}{(\varepsilon_r k_z)^2 - ((k_{1z})_R)^2} H_1^{(2)}(k_\rho\rho) + k_0^2 \int_{-\infty}^{\mathrm{Im}k_1} j\,dk_\rho'' \frac{2k_\rho (k_{1z})_R}{k_z^2 - ((k_{1z})_R)^2} H_1'^{(2)}(k_\rho\rho)\right\}. \tag{17}$$

The criterion of deciding the sign of the square root of k_z and k_{1z} is the same as in the evaluation of $W_\rho(\rho)$. Also note that the half-space solution is only a function of ρ and k_1/k_0. They can be computed and tabulated. We integrate W_ρ^N numerically along the Sommerfeld integration path as in Fig. 2. For W_ρ^H, the integration is given as (13) and (14) starting from $k_\rho'' = -|k_{\rho\max}''|$. We use $k_{\rho\max}'' = 40/\rho$ and $\Delta k_\rho'' = \min(0.1k_{\rho\max}'', 0.05/\rho, 0.01k_0)$.

IV. Evaluation of Electric Field Spatial Green's Function Using Higher Order Asymptotic Extraction

In the following the results of higher order asymptotic extraction are summarized [15], [16]. The important convergence comes from subtracting out the leading two orders of k_ρ dependence. Thus, $W_\rho(\rho)$ of (3) is decomposed as follows:

$$W_\rho(\rho) = W_\rho^{(P)}(\rho) + W_\rho^{(RA)}(\rho) + W_\rho^{(RN)}(\rho) \tag{18}$$

where

$$W_\rho^{(RN)}(\rho) = \frac{1}{4\pi\omega\varepsilon_0}\int_{C_s} dk_\rho \cdot \left\{k_\rho k_z R_{\mathrm{TM}} J_1'(k_\rho\rho) - F_\rho(k_\rho, z=0) - \frac{k_0^2}{\rho} R_{\mathrm{TE}} \frac{J_1(k_\rho\rho)}{k_z}\right\} \tag{19}$$

$$F_\rho(k_\rho, z) = \left[-k_\rho k_z K J_0(k_\rho\rho) - \frac{jk_\rho K}{\rho} J_1(k_\rho\rho) + \frac{jKk_0^2\varepsilon_r}{(1+\varepsilon_r)} J_1'(k_\rho\rho)\right] e^{-k_\rho z} \tag{20}$$

$$K = \frac{\varepsilon_r - 1}{\varepsilon_r + 1}.$$

In (18), (P) stands for "primary wave," (RA) stands for "response analytical," and (RN) stands for "response numerical." The primary wave is the analytic result of the spatial Green's function in free-space, the "response analytical" is the part of the response of the asymptotic extraction and has an analytical result. The "response numerical" is the part of the response that is to be evaluated numerically

$$W_\rho^{(P)}(\rho) = \frac{1}{4\pi\omega\varepsilon_0}\frac{je^{-jk\rho}}{\rho}\left(-\frac{2jk_0}{\rho} - \frac{2}{\rho^2}\right) \tag{21}$$

$$W_\rho^{(RA)}(\rho) = \frac{1}{4\pi\omega\varepsilon_0}\left\{-\frac{jK}{\rho}\left(\frac{1}{\rho^2} + \frac{jk_0}{\rho}\right) - \frac{jK}{\rho^3}\right\}. \tag{22}$$

The integrand with higher order asymptotic extraction decays as $k_\rho^{-3/2}$ when k_ρ is large. We integrate $W_\rho^{(RN)}$ numerically along the Sommerfeld integration path. The Green's function $W_\phi(\rho)$ can be calculated in a similar manner

$$W_\phi(\rho) = W_\phi^{(P)}(\rho) + W_\phi^{(RA)}(\rho) + W_\phi^{(RN)}(\rho) \tag{23}$$

where

$$W_\phi^{(RN)}(\rho) = \frac{1}{4\pi\omega\varepsilon_0}\int_{C_s} dk_\rho \cdot \left\{\left(-\frac{1}{\rho}\right)[k_z R_{\mathrm{TM}} J_1(k_\rho\rho) - F_\phi(k_\rho, z=0)] + k_0^2 \frac{k_\rho}{k_z} R_{\mathrm{E}} J_1'(k_\rho\rho)\right\} \tag{24}$$

$$F_\phi(k_\rho, z) = \left[jk_\rho K J_1(k_\rho\rho) - j\frac{k_0^2 K^2}{2k_\rho} J_1(k_\rho\rho)\right] e^{-k_\rho z} \tag{25}$$

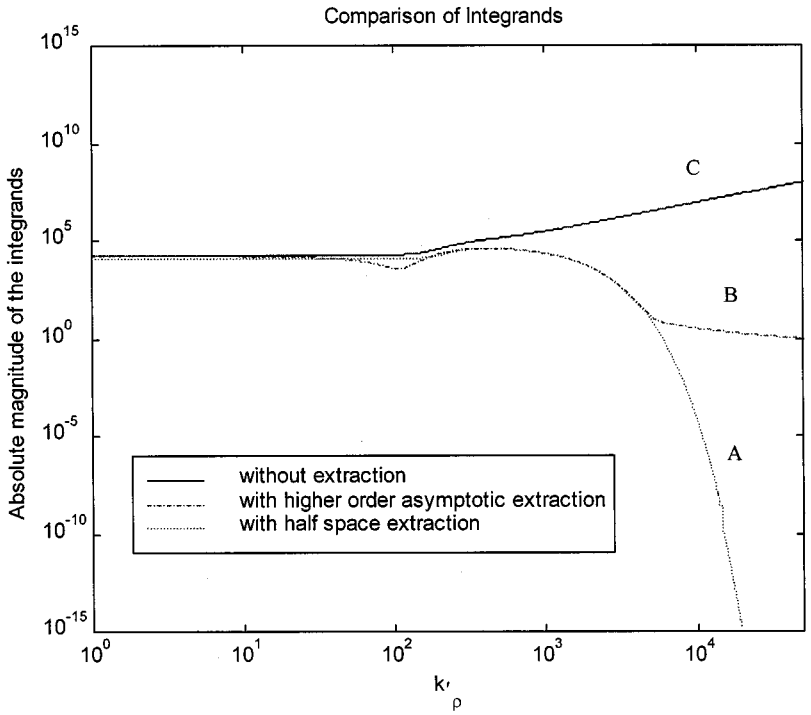

Fig. 4. Absolute values of the integrand A with half-space extraction, the integrand B with the higher order extraction and the integrand C without the extraction as a function of k'_ρ in m^{-1}. A log–log scale is used showing the exponential decay in A and power-law dependence in B and inverse power-law dependence in C for large k'_ρ. The parameters are: frequency = 8 GHz, $\varepsilon_1 = 2\varepsilon_0, \varepsilon_2 = 4\varepsilon_0, \varepsilon_3 = 7\varepsilon_0, \varepsilon_4 = 11\varepsilon_0$ and $h_1 = h_2 = h_3 = 0.0013$ m. The integrands are on C_2 of the Sommerfeld integration path with $k''_\rho = 76.923\ \mathrm{m}^{-1}$. Also $\rho = 1.5\lambda$.

and the analytic results of $W_\phi^{(P)}(\rho)$ and $W_\varphi^{(RA)}$ are as follows:

$$W_\phi^{(P)}(\rho) = \frac{j}{4\pi\omega\varepsilon_0}\frac{e^{-jk\rho}}{\rho}\left(k_0^2 - \frac{jk_0^2}{\rho} - \frac{1}{\rho^2}\right) \tag{26}$$

is the primary field

$$W_\phi^{(RA)} = \frac{1}{4\pi\omega\varepsilon_0}\left(-\frac{1}{\rho}\right)\left(\frac{jK}{\rho^2} - \frac{jK^2k_0^2}{2}\right) \tag{27}$$

is the analytical response due to asymptotic extraction.

V. Results of Surface Electric Fields Based on Half-Space Extraction and on Higher Order Asymptotic Extraction

In Fig. 4, we plot the integrand of $W_\rho(\rho)$ with half-space extraction, higher order asymptotic extraction and without any extraction. We plot the magnitudes of the integrands along C_2 of the Sommerfeld path as a function of k'_ρ on a log–log scale. The integrands are

$$A = \frac{1}{4\pi\omega\varepsilon_0}\left\{k_\rho k_z(R_{01}^{\mathrm{TM}} - R_{\mathrm{TM}})J_1'(k_\rho\rho) + \frac{k_0^2}{\rho}(R_{\mathrm{TE}} - R_{01}^{\mathrm{TE}})\frac{J_1(k_\rho\rho)}{k_z}\right\} \tag{28}$$

$$B = \frac{1}{4\pi\omega\varepsilon_0}\cdot\left\{(k_\rho k_z R_{\mathrm{TM}}J_1'(k_\rho\rho) - F_\rho(k_\rho)) - \frac{k_0^2}{\rho}R_{\mathrm{TE}}\frac{J_1(k_\rho\rho)}{k_z}\right\} \tag{29}$$

$$C = \frac{1}{4\pi\omega\varepsilon_0}\left\{(k_\rho k_z R_{\mathrm{TM}}J_1'(k_\rho\rho)) - \frac{k_0^2}{\rho}R_{\mathrm{TE}}\frac{J_1(k_\rho\rho)}{k_z}\right\} \tag{30}$$

A is the integrand of $W_\rho(\rho)$ with the half-space extraction. B is the integrand of $W_\rho(\rho)$ with the higher order asymptotic extraction, and C is the integrand without any extraction. For large k'_ρ, the figure shows that the integrand A with the half-space extraction decays exponentially, the integrand B with higher order asymptotic extraction decays as $k_\rho^{-3/2}$. On the other hand, the integrand C without extraction grows with $k_\rho^{3/2}$. Note that along C_2, k'_ρ is equal to $k''_{\rho\max}$ so that the denominator of R_{TM} is never equal to zero. The peak of the integrand occurs when the path is close to the surface wave pole. Also, for large k_ρ, the function B and C of Fig. 4 on the log–log scale asymptotically approach straight lines showing the power-law dependence of the growth of B and the inverse power-law dependence of C. The case we illustrate is four layers with $\varepsilon_1 = 2\varepsilon_0$, $\varepsilon_2 = 4\varepsilon_0$, $\varepsilon_3 = 7\varepsilon_0$, and $\varepsilon_4 = 11\varepsilon_0$. Next, we plot the numerical results of W_ρ and W_ϕ using half-space extraction and higher order asymptotic extraction respectively. Because of the large magnitude differences in the distance range between 0.02λ to 1.5λ where λ is the free-space wavelengths, we plot the results separately for the real and the imaginary parts and for two distances ranges to show more clearly the results which exhibit wave-like behavior as a function of distance. We plot the numerical results of the electric field spatial Green's functions W_ρ and W_ϕ as a function of ρ from 0.02λ to 0.2λ. In this distance range, the magnitude

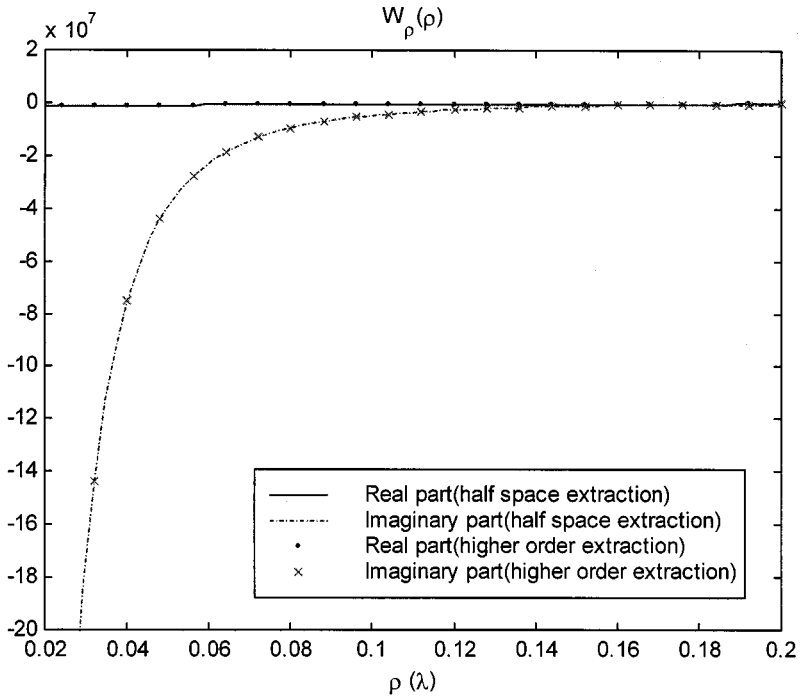

Fig. 5. The real part and imaginary part of surface electric fields of spatial Green's functions as a function of distance ρ in wavelengths $(0.02\lambda - 0.2\lambda)$. The parameters are: frequency $= 8$ GHz; $\varepsilon_1 = 2\varepsilon_0$; $\varepsilon_2 = 4\varepsilon_0$; $\varepsilon_3 = 7\varepsilon_0$; $\varepsilon_4 = 11\varepsilon_0$; $h_1 = h_2 = h_2 = 0.0013$ m.

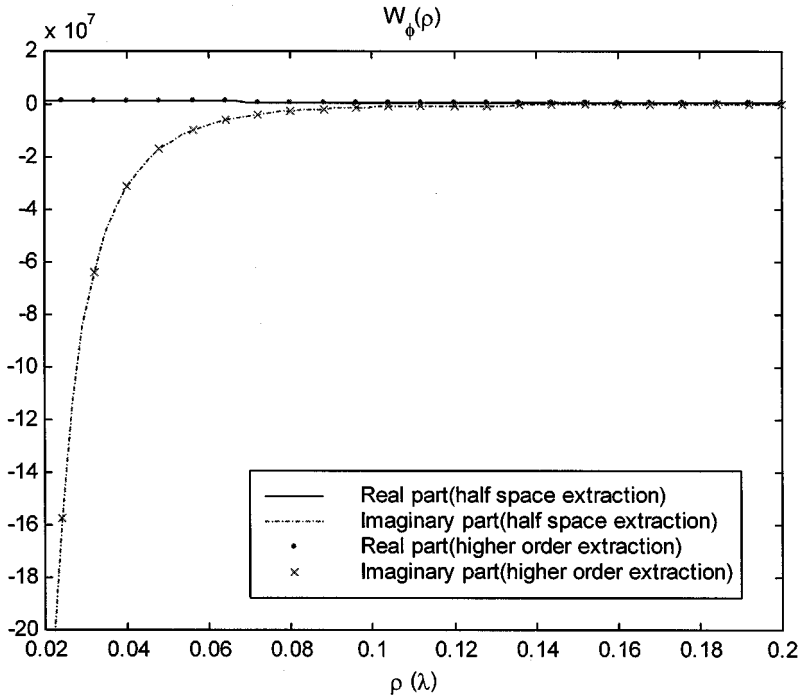

Fig. 6. The real part and imaginary part of surface electric fields of spatial Green's functions as a function of distance ρ in wavelengths $(0.02\lambda - 0.2\lambda)$. The parameters are: frequency $= 8$ GHz; $\varepsilon_1 = 2\varepsilon_0$; $\varepsilon_2 = 4\varepsilon_0$; $\varepsilon_3 = 7\varepsilon_0$; $\varepsilon_4 = 11\varepsilon_0$; $h_1 = h_2 = h_2 = 0.0013$ m.

of the imaginary parts are much larger than the magnitude of the real parts. The results are shown in Figs. 5 and 6. In Figs. 7 and 8, we show W_ρ and W_ϕ as a function of ρ from 0.02λ to 1.5λ. In this distance range, the spatial Green's functions $W_\rho(\rho)$ and $W_\phi(\rho)$ show interference wave patterns. Note that the results of half-space extraction and higher order asymptotic extraction are in good agreement, as shown in Figs. 5–8.

VI. Comparison of Results of Impedance Matrix Elements Between Surface Electric Field Green's Function Method and Spectral Domain Method

To validate the solution of the computed surface electric field, we compare the results of impedance matrix element between the present method of the surface electric field spatial

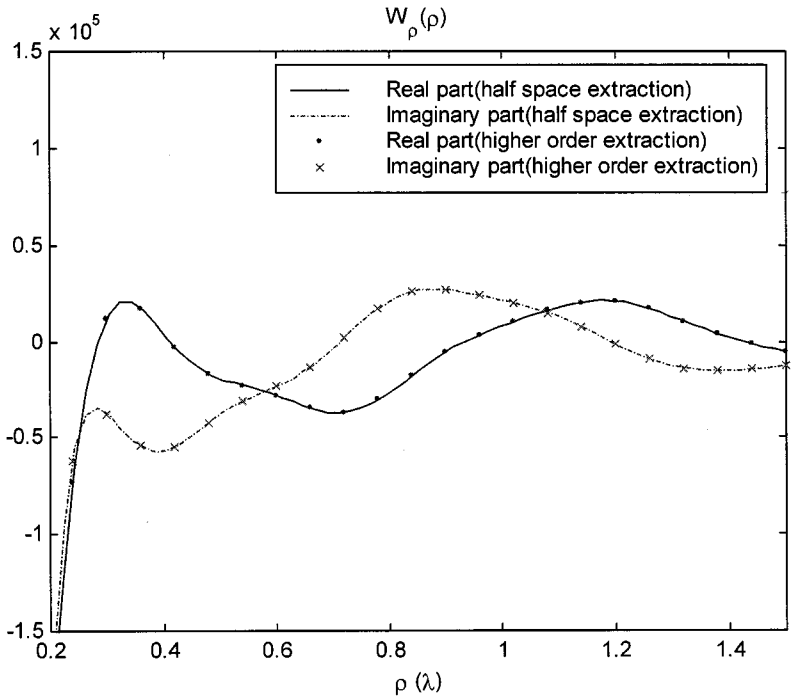

Fig. 7. The real part and imaginary part of surface electric fields of spatial Green's functions as a function of distance ρ in wavelengths $(0.2\lambda - 1.5\lambda)$. The parameters are: frequency $= 8$ GHz; $\varepsilon_1 = 2\varepsilon_0$; $\varepsilon_2 = 4\varepsilon_0$; $\varepsilon_3 = 7\varepsilon_0$; $\varepsilon_4 = 11\varepsilon_0$; $h_1 = h_2 = h_2 = 0.0013$ m.

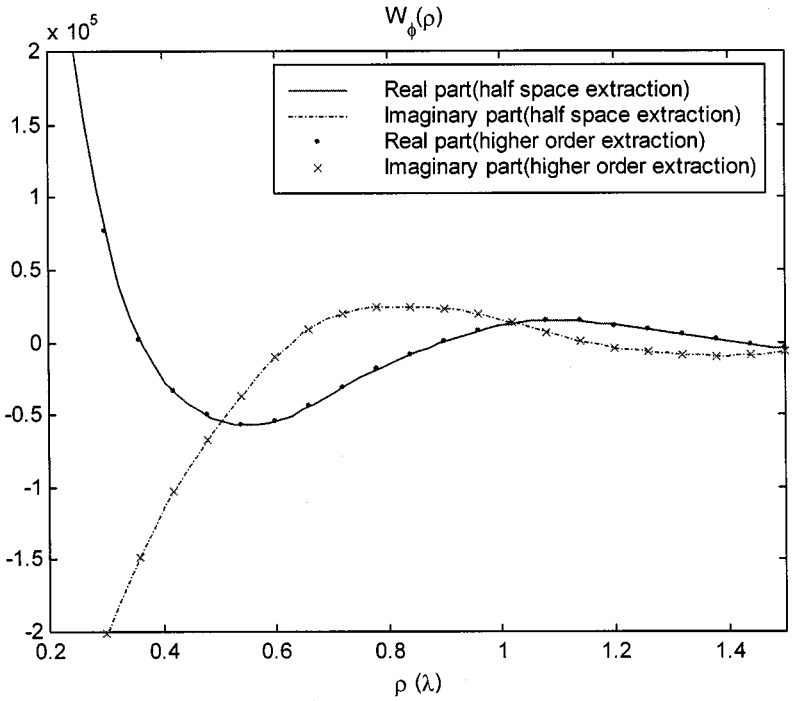

Fig. 8. The real part and imaginary part of surface electric fields of spatial Green's functions as a function of distance ρ in wavelengths $(0.2\lambda - 1.5\lambda)$. The parameters are: frequency $= 8$ GHz; $\varepsilon_1 = 2\varepsilon_0$; $\varepsilon_2 = 4\varepsilon_0$; $\varepsilon_3 = 7\varepsilon_0$; $\varepsilon_4 = 11\varepsilon_0$; $h_1 = h_2 = h_2 = 0.0013$ m.

(SEFS) Green's function method and the spectral domain method [14]. The impedance elements are important steps to solve integral equations for antenna radiation on the surface of stratified media.

In the method of moments solution, the impedance matrix element relates the "interaction" of the jth patch (field) and the ith patch (source). The impedance matrix element in the spatial domain is

$$Z_{xx}^{ji} = \iint\limits_{j\text{th}\,patch} dx\,dy w_j(x, y)$$

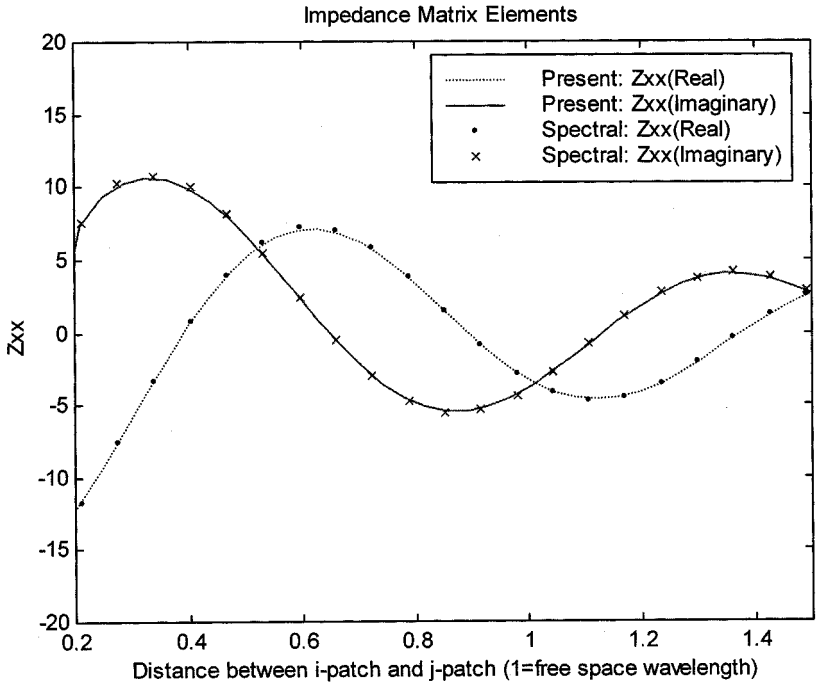

Fig. 9. The real part and imaginary part of impedance matrix elements $Z_{xx}^{ji}/(\Delta x)^2(\Delta y)$ along the x-axis, as determined by source current direction using spatial domain method and spectral domain method. The other parameters are: frequency $= 8$ GHz; $\varepsilon_1 = 10.65\varepsilon_0$; $h_1 = 0.0013$ m; $\Delta x,\ \Delta y = 0.00024$ m; $\lambda = 0.0375$ m; $x_x^{(i)} = y_x^{(i)} = y_x^{(j)} = 0$.

$$\cdot \iint\limits_{i\text{th}patch} dx'\, dy' G_{xx}(x-x',\, y-y') b_i(x',\, y') \quad (31)$$

where the basis functions b_i and the testing functions w_j are nonzero only on the ith patch and the jth patch, respectively. The center of the ith patch is at $(x_i,\, y_i)$ and the center of the jth patch is at $(x_j,\, y_j)$. We use Galerkin's method and rooftop for both testing and basis functions. Equation (31) becomes

$$Z_{xx}^{ji} = \int_{x_j-\Delta x}^{x_j+\Delta x} dx \int_{x_i-\Delta x}^{x_i+\Delta x} dx' \int_{y_j-(\Delta y/2)}^{y_j+(\Delta y/2)} dy \cdot \int_{y_i-(\Delta y/2)}^{y_i+(\Delta y/2)} dy' t_{x_j}(x) \cdot t_{x_i}(x') \cdot G_{xx}(x-x',\, y-y') \quad (32)$$

where

$$t_{x_j}(x) = \begin{cases} 1 - \dfrac{|x-x_j|}{\Delta x}, & \text{for } |x-x_j| \le \Delta x \\ 0, & \text{elsewhere} \end{cases} \quad (33)$$

$$t_{x_i}(x') = \begin{cases} 1 - \dfrac{|x'-x_i|}{\Delta x}, & \text{for } |x'-x_i| \le \Delta x \\ 0, & \text{elsewhere.} \end{cases} \quad (34)$$

Based on the computed and tabulated $W_\rho(\rho)$ and $W_\phi(\rho)$, $G_{xx}(x-x',\, y-y')$ can be calculated easily. These are then used to calculate the impedance matrix elements as given in equation (32) with rooftop testing and basis functions. The integrals in (32) are done by using three-point quadratures for each integral dx, dx', dy and dy'. The results are denoted as SEFS method (present method). For self patch and overlap patch, the calculation of the impedance matrix elements are given in Appendix II. A common method of calculating the impedance matrix elements for many years is the spectral domain method [14]. We next compare (32) based on the present method with the impedance matrix elements using this common spectral domain method with the same rooftop testing functions and basis functions as before. For the spectral domain method, the impedance matrix element is

$$Z_{xx}^{ji} = \frac{1}{4\pi^2} \iint\limits_{-\infty}^{\infty} dk_x\, dk_y \tilde{w}_x^{(j)}(-k_x,\, -k_y) \cdot \tilde{G}_{xx}(k_x,\, k_y) \tilde{b}_x^{(i)}(k_x,\, k_y) \quad (35)$$

where

$$\tilde{G}_{xx}(k_x,\, k_y) = \frac{-\omega\mu}{2k_z} \left\{ \frac{k_y^2}{k_\rho^2}(1+R_{\text{TE}}) + \frac{k_z^2 k_x^2}{k^2 k_\rho^2}(1-R_{\text{TM}}) \right\} \quad (41)$$

$$\tilde{w}_x(k_x,\, k_y) = e^{-jk_x(\Delta x + x_j)} \frac{\sin^2\left(\dfrac{\Delta x}{2}k_x\right)}{\left(\dfrac{k_x}{2}\right)^2 \Delta x} \cdot e^{-jk_y((\Delta y/2)+y_j)} \frac{2\sin\left(\dfrac{\Delta y}{2}k_y\right)}{k_y} \quad (42)$$

TABLE I
THE REAL PART AND THE IMAGINARY PART OF IMPEDANCE MATRIX ELEMENTS $Z_{xx}^{ji}/(\Delta x)^2(\Delta y)$ ALONG THE x-AXIS AS DETERMINED BY SOURCE CURRENT DIRECTION. FOR PERCENTAGE DIFFERENCE IN THE LAST COLUMN, WE USE THE FORMULA $|(Z_1 - Z_2)/Z_2|$ WHERE Z_1 REPRESENTS THE VALUES USING THE SEFS METHOD AND Z_2 REPRESENTS THE VALUES USING THE SPECTRAL DOMAIN METHOD. THE OTHER PARAMETERS ARE: FREQUENCY = 8 GHz; $\varepsilon_1 = 10.65\varepsilon_0$; $h_1 = 0.0013$ M; Δx, $\Delta y = 0.00024$ M; $\lambda = 0.0375$ M; $x_x^{(i)} = y_x^{(i)} = y_x^{(j)} = 0$

	Spectral Domain Method		Present Method		
Patches separation n $(n\Delta x)$	Real part	Imaginary part	Real part	Imaginary part	Percentage difference(%)
0	-2.09E+01	1.97E+06	0.00E+00	1.98E+06	0.60%
1	-1.84E+01	-6.78E+05	0.00E+00	-6.71E+05	0.98%
3	-1.902E+01	-4.896E+04	-1.893E+01	-4.870E+04	0.52%
13	-1.783E+01	-4.249E+02	-1.776E+01	-4.239E+02	0.25%
23	-1.531E+01	-1.560E+01	-1.525E+01	-1.580E+01	0.99%
33	-1.182E+01	7.558E+00	-1.179E+01	7.522E+00	0.32%
43	-7.621E+00	1.028E+01	-7.601E+00	1.023E+01	0.40%
53	-3.290E+00	1.078E+01	-3.282E+00	1.073E+01	0.43%
63	7.057E-01	9.987E+00	7.021E-01	9.943E+00	0.44%
73	3.953E+00	8.100E+00	3.941E+00	8.065E+00	0.41%
83	6.155E+00	5.433E+00	6.136E+00	5.411E+00	0.36%
93	7.161E+00	2.404E+00	7.136E+00	2.394E+00	0.35%
103	6.976E+00	-5.436E-01	6.951E+00	-5.508E-01	0.37%
113	5.768E+00	-3.047E+00	5.743E+00	-3.030E+00	0.46%
123	3.810E+00	-4.766E+00	3.794E+00	-4.745E+00	0.44%
133	1.478E+00	-5.555E+00	1.469E+00	-5.528E+00	0.49%
143	-8.476E-01	-5.383E+00	-8.520E-01	-5.355E+00	0.51%
153	-2.818E+00	-4.366E+00	-2.820E+00	-4.344E+00	0.43%
163	-4.167E+00	-2.737E+00	-4.167E+00	-2.724E+00	0.27%
173	-4.736E+00	-8.047E-01	-4.735E+00	-7.994E-01	0.11%
183	-4.496E+00	1.106E+00	-4.500E+00	1.103E+00	0.11%
193	-3.547E+00	2.701E+00	-3.559E+00	2.685E+00	0.46%
203	-2.099E+00	3.747E+00	-2.113E+00	3.716E+00	0.79%
213	-4.122E-01	4.145E+00	-4.286E-01	4.070E+00	1.86%
223	1.239E+00	3.774E+00	1.209E+00	3.734E+00	1.26%
233	2.567E+00	2.839E+00	2.537E+00	2.807E+00	1.15%

$$\tilde{b}_x(k_x, k_y) = e^{-jk_x(\Delta x + x_i)} \frac{\sin^2\left(\frac{\Delta x}{2}k_x\right)}{\left(\frac{k_x}{2}\right)^2 \Delta x} \cdot e^{-jk_y((\Delta y/2)+y_i)} \frac{2\sin\left(\frac{\Delta y}{2}k_y\right)}{k_y}. \tag{43}$$

Note that $\tilde{w}_x$ and $\tilde{b}_x$decay for large k_ρ. In the calculation, we let $k_x = k_\rho \cos\phi_k$, $k_y = k_\rho \sin\phi_k$ and $\int dk_x \int dk_y = \int_{C_s} dk_\rho k_\rho \int_0^{2\pi} d\phi_k$. For the $d\phi_k$ integration, we use $\Delta\phi_k = (2\pi)/5000$. The evaluation of k_ρ integral is carried along the Sommerfeld integral path, as in Fig. 2, using the following numerical parameters: $\Delta k'_\rho = 0.005 * k_0$, $k'_{\rho\max} = 30/h$, and $k''_{\rho\max} = 0.1/h$.

In the following, we compare and tabulate the results of the impedance matrix elements using the present method and spectral domain method for a two-layer case $\varepsilon_1 = 10.65\varepsilon_0$, ε_2 is a perfect electric conductor, frequency = 8 GHz and $h_1 = 0.0013\ \mathrm{m} = 0.0347\lambda$. In Fig. 9, we show the normalized impedance matrix elements $Z_{xx}^{ji}/(\Delta x)^2(\Delta y)$ with the jth patch centered at $(x_x^{(j)}, y_x^{(j)})$ and the ith patch centered at $(x_x^{(i)}, y_x^{(i)})$. We illustrate results for the cases of $x_x^{(i)} = y_x^{(i)} = y_x^{(j)} = 0$ and variable $x_x^{(j)}$. The $x_x^{(j)}$ assume discrete values based on the cell sizes Δx and $x_x^{(j)} = n\Delta x$ where $n = 0, 1, 3, 10, \cdots$ up to 233. Each cell has the dimensions of Δx by Δy where $\Delta x = \Delta y = 0.00024\ \mathrm{m} = 0.0064\lambda$. The Fig. 9 shows that there is a good agreement between this method and spectral domain method. In Table I, the results of the normalized impedance matrix using spatial domain method and spectral domain method are tabulated and the percentage difference between two methods is shown in the last column. The percentage difference is $|(Z_1 - Z_2)/Z_2|$ where Z_1 is the value using SEFS (this) method and Z_2 is the value of spectral domain method. It shows that the difference between two methods is less than 2% for the whole range from 0 to 1.5λ. Note that the first row and second row of the tables are the self patch and overlap patch, respectively. The calculation of these two rows are given in Appendix I.

VII. CONCLUSION

In this paper, we calculated the surface electric field Green's function for stratified media in the spatial domain with field and source points on the same interface surface dividing stratified media. Numerical calculations are performed by numerically

carrying out the integration along the Sommerfeld integration path and using half-space extraction. The half-space extraction part is calculated by numerical integration along the vertical branch cuts. Surface electric fields for the stratified media are computed directly without the use of the potentials and without the need for location of poles. The computed values are computed as a function of distance range from 0.02 free-space wavelengths to 1.5 free-space wavelengths. To validate the accuracy of the solution, we also compute the impedance matrix elements using surface electric field, testing, and basis functions all in spatial domain. The results are then compared with the results of the spectral domain method. The comparisons are tabulated and show that the difference is less than 2%. Solutions for distance larger that 1.5 free-space wavelengths and derivatives may be calculated by asymptotic method [1]–[4], [21]–[23].

APPENDIX I

The integral identities are obtained by using Sommerfeld integral. Derivative of these integrals are then taken with respect to $\rho$and/or z and then the limit $z = 0^+$ is taken.

The Sommerfeld integral identify is

$$I_s(\rho, z, k) = \int_{C_s} dk_\rho \frac{k_\rho}{k_z} e^{-jk_z z} J_0(k_\rho \rho) = j\frac{e^{-jkr}}{r} \quad \text{where } r = \sqrt{\rho^2 + z^2}. \tag{A.1}$$

If we differentiate (A.1) twice with respect to z and then take $z \to 0^+$, we have

$$\lim_{z\to 0^+} \frac{d^2}{dz^2} \int_{C_s} dk_\rho \frac{k_\rho}{k_z} J_0(k_\rho \rho)\, e^{-jk_z z} = -\lim_{z\to 0^+} \int_0^\infty dk_\rho k_\rho k_z J_0(k_\rho \rho) e^{-jk_z z} = \left(\frac{k}{\rho^2} - \frac{j}{\rho^3}\right) e^{-jk\cdot\rho}. \tag{A.2}$$

APPENDIX II

In the calculation of self-patch and overlap-patch impedance matrix, we use electrostatic approximation for the electric field Green's function in the near field.

Thus, we have

$$G_{xx}(x - x', 0) = -\frac{j(1+K)}{4\pi\omega\varepsilon_0} \frac{\partial^2}{\partial x \partial x'} \frac{1}{\rho} \quad \text{where } K = \frac{\varepsilon_r - 1}{\varepsilon_r + 1}. \tag{A.3}$$

The calculation of the impedance matrix for the case of self-patch and overlap-patch case are given as follows:

1) self-patch ($|x_i - x_j| = 0$):

$$Z_{xx}^{jj} = Z_{xx}^{(N)jj} + Z_{xx}^{(A)jj}$$

where

$$Z_{xx}^{(N)jj} = \frac{j(1+K)}{\pi\omega\varepsilon_0(\Delta x)^2} \left(\int_0^{\Delta x} dx \int_0^{\Delta x} dx' I_p(x, x') - \int_0^{\Delta x} dx \int_{-\Delta x}^{0} dx' I_p(x, x') \right)$$

$$I_p(x, x') = \Delta y \ln\left(\Delta y + \sqrt{(x - x')^2 + (\Delta y)^2}\right) - \sqrt{(x - x')^2 + (\Delta y)^2} + |x - x'|$$

$$Z_{xx}^{(A)jj} = \frac{2j(1+K)\Delta y}{\pi\omega\varepsilon_0} (\ln(2\Delta x) - \ln(\Delta x)) \tag{A.4}$$

2) overlap-patch ($|x_i - x_j| = \Delta x$)

$$Z_{xx}^{ji} = Z_{xx}^{(N)ji} + Z_{xx}^{(A)ji}$$

where

$$Z_{xx}^{(N)ji} = \frac{j(1+K)}{\pi\omega\varepsilon_0(\Delta x)^2} \left\{ \int_0^{\Delta x} dx \int_{-\Delta x}^{0} dx' I_p(x, x') + \int_{\Delta x}^{2\Delta x} dx \int_0^{\Delta x} dx' I_p(x, x') - \int_{\Delta x}^{2\Delta x} dx \int_{-\Delta x}^{0} dx' I_p(x, x') - \int_0^{\Delta x} dx \int_0^{\Delta x} dx' I_p(x, x') \right\}$$

$$Z_{xx}^{(A)ji} = \frac{j(1+K)\Delta y}{2\pi\omega\varepsilon_0} \left\{ \frac{7}{2}\ln(\Delta x) - 8\ln(2\Delta x) + \frac{9}{2}\ln(3\Delta x) \right\}. \tag{A.5}$$

REFERENCES

[1] J. R. Wait, *Electromagnetic Waves in Stratified Media*. New York: Pergamon, 1970.

[2] ——, "Characteristics of antennas over lossy earth," in *Antenna Theory*, R. E. Collin and F. J. Zucker, Eds. New York: McGraw-Hill, 1969, pp. 387–437.

[3] J. A. Fuller and J. R. Wait, "A pulsed dipole in the Earth," in *Transient Electromagnetic Fields*, L. B. Felsen, Ed. New York: Springer-Verlag, 1976, pp. 237–269.

[4] J. R. Wait, *Geo Electromagnetics*. New York: Academic, 1982.

[5] A. Banos, *Dipole Radiation in the Presence of a Conducting Half Space*. New York: Pergamon, 1966.

[6] L. Tsang, R. Brown, J. A. Kong, and G. Simmons, "Numerical evaluation of electromagnetic fields due to dipole antennas in the presence of stratified media," *J. Geophys. Res.*, vol. 17, pp. 2077–2080, May 1974.

[7] L. Tsang and D. Rader, "Numerical evaluation of transient acoustic waveform due to a point source in a fluid-filled borehole," *Geophys.*, vol. 44, no. 10, pp. 1706–1720, Oct. 1979.

[8] K. A. Michalski and J. R. Mosig, "Multilayered media Green's functions in integral equation formulations," *IEEE Trans. Antennas Propagat.*, vol. 45, pp. 508–519, Mar. 1997.

[9] J. R. Mosig, "Integral equation technique," in *Numerical Techniques for Microwave and Millimeter-Wave Passive Structures*, T. Itoh, Ed. New York: Wiley, 1989, ch. 3, pp. 113–213.

[10] D. G. Fang, J. J. Yang, and G. Y. Delisle, "Discrete image theory for horizontal electric dipoles in a multilayered medium," *Proc. Inst. Elect. Eng. (Microwaves, Antennas, Propagat.)*, pt. H, vol. 135, no. 5, pp. 297–303, Oct. 1988.

[11] Y. L. Chow, J. J. Yang, D. G. Fang, and G. E. Howard, "A closed form spatial green's function for the thick microstrip substrate," *IEEE Trans. Microwave Theory Tech.*, vol. 39, pp. 588–592, Mar. 1991.
[12] R. A. Kipp and C. H. Chan, "Complex image method for sources in bounded regions of multi-layer structures," *IEEE Trans. Microwave Theory Tech.*, vol. 42, pp. 860–865, May 1994.
[13] ——, "A complex image method for the vertical component of the magnetic potential of a horizontal dipole in layered media," in *Proc. IEEE AP-S Int. Conf.*, vol. 2, Seattle, WA, June 1994, pp. 1366–9.
[14] D. M. Pozar, "Input impedance and mutual coupling of rectangular microstrip antennas," *IEEE Trans. Antennas Propagat.*, vol. AP-30, pp. 1191–1196, Nov. 1982.
[15] L. Tsang, "Near-field radiation from microstrip lines," *Microwave Opt. Technol. Lett.*, vol. 19, no. 3, pp. 176–184, 1998.
[16] L. Tsang, J. H. Cha, and J. R. Thomas, "Electric fields of spatial Green's functions of microstrip structures and applications to the calculations of impedance matrix elements," *Microwave Opt. Technol. Lett.*, vol. 20, no. 2, pp. 90–97, Jan. 1999.
[17] A. Sommerfeld, *Partial Differential Equations in Physics*. New York: Academic, 1964.
[18] E. K. Miller, A. J. Poggio, G. J. Burke, and E. S. Selden, "Analysis of wire antennas in the presence of a conducting half-space," *Can. J. Phys.*, vol. 50, no. 9, pp. 879–88, May 1972.
[19] J. L. Tsalamengas, "TE-scattering by conducting strips right on the planar interface of a three-layered medium," *IEEE Trans. Antennas Propagat.*, vol. 41, pp. 1650–8, Dec. 1993.
[20] K. A. Michalski, *Moment Methods in Antennas and Scattering*, R. C. Hansen, Ed. Norwood, MA: Artech House, 1990.
[21] J. A. Kong, *Electromagnetic Wave Theory*. New York: Wiley, 1986.
[22] L. Tsang, J. A. Kong, and R. Shin, *Theory of Microwave Remote Sensing*. New York: Wiley, 1985.
[23] W. C. Chew, *Waves and Fields in Inhomogeneous Media*. New York: Van Nostrand Reinhold, 1995.
[24] L. Tsang, C. C. Huang, and C. H. Chan, "Surface electric fields and spatial derivatives of Green's function of layered media based on half space extraction," *Microwave Opt. Technol. Lett.*, vol. 24, no. 4, pp. 247–253, Feb. 2000.

Leung Tsang (S'73–M'75–SM'85–F'90) was born in Hong Kong. He received the B.S., M.S., E.E., and Ph.D. degrees, all from the Massachusetts Institute of Technology, Cambridge, in 1971, 1973, and 1976, respectively.

He is currently a Professor of electrical engineering at the University of Washington, Seattle. He is a coauthor of *Theory of Microwave Remote Sensing* (New York: Wiley, 1985). His current research interests include wave propagation in random media and rough surfaces, remote sensing, optoelectronics, and computational electromagnetics.

Dr. Tsang has been the Editor-in-Chief of IEEE TRANSACTIONS ON GEOSCIENCE AND REMOTE SENSING since 1996. He was the Technical Program Chairman of the 1994 IEEE Antennas and Propagation International Symposium and URSI Radio Science Meeting and the Technical Program Chairman of the 1995 Progress in Electromagnetics Research Symposium. He was the General Chairman of the 1998 IEEE International Geoscience and Remote Sensing Symposium. He is a Fellow of the Optical Society of America.

Chung-Chi Huang, photograph and biography not available at time of publication.

Chi Hou Chan received the Ph.D. degree in electrical engineering from the University of Illinois, Urbana, in 1987.

From 1987 to 1989, he was a Visiting Assistant Professor at the University of Illinois associated with the Electromagnetic Communication Laboratory. He joined the Department of Electrical Engineering at the University of Washington, Seattle, in 1989 as an Assistant Professor and was promoted to Associate Professor (with tenure) in 1993. Since April 1996, he has been with the Department of Electronic Engineering, City University of Hong Kong, where he is currently Professor (Chair) of Electronic Engineering, Group I (Electronic Engineering) Leader, and Associate Dean of Faculty of Science and Engineering. From July 1996 to June 1998, he also served as the Director of the Applied Electromagnetics Laboratory in the Electrical Engineering Department at the same university. His research interests have been in computational electromagnetics and its applications.

Dr. Chan is the recipient of the 1991 U.S. National Science Foundation Presidential Young Invesitgator Award. He is a Fellow of CIE and the Institute of Electrical Engineering.